Highly collimated emission from a left-handed photonic crystal with a quasi-cavity

Article *in* Applied Physics B · September 2009

DOI: 10.1007/s00340-009-3649-y

4 authors, including:

Wenyao Liang
South China University of Technology
13 PUBLICATIONS **86** CITATIONS
SEE PROFILE

Jian-Wen Dong
Sun Yat-Sen University
90 PUBLICATIONS **890** CITATIONS
SEE PROFILE

Appl Phys B (2009) 96: 781–785
DOI 10.1007/s00340-009-3649-y

Applied Physics B
Lasers and Optics

Highly collimated emission from a left-handed photonic crystal with a quasi-cavity

W.Y. Liang · J.W. Dong · G.Q. Liang · H.Z. Wang

Received: 14 June 2008 / Revised version: 18 May 2009 / Published online: 18 July 2009

Abstract We study the collimated emission characteristics from a dipole source inside a negative-effective-refractive-index photonic crystal with a quasi-cavity constructed by a concave photonic crystal reflector. The emissions along the $\pm X$ and $-Y$ directions are forbidden by the quasi-cavity, so that most emissions propagate along the $+Y$ direction. Simulation results show that a narrow collimated beam is achieved due to the near-zero negative effective refractive index. Moreover, the half-power beam width of such a collimated beam can be reduced to 3.48° by optimizing the size of the source area. Such a compact structure would have potential applications in micro-optical devices.

PACS 42.70.Qs · 42.25.Gy · 41.20.Jb

1 Introduction

Photonic crystals (PCs), which are periodic dielectric or metallo-dielectric structures, have many interesting properties such as a photonic band gap (PBG) and anomalous refraction effects, and they have a wide range of applications, from microwave to optical frequencies [1–24]. Methods and technologies to achieve a well collimated electromagnetic (EM) beam, i.e., directional emission (DE), have always been attractive for their significant practical applications [4–19], e.g., coupling EM wave out of PC devices into conventional optical systems or free space in an efficient manner. DE was first demonstrated by Lezec et al. [4] through a single metal aperture surrounded by periodic surface corrugations. Later, DEs were extended to PC waveguides, which are implemented by using surface modification, introducing point defects into the output surface, or using a partial photonic band gap (PBG) and so on [5–15]. In order to achieve high-efficiency coupling, a strictly precise alignment between the input beam and the narrow PC waveguide is necessary. These methods were realized from PC structures with positive dispersion relations. Recently, self-collimation-based DEs related to negative dispersion relations of PCs were reported. For such DEs [16–18], the alignment mentioned above is unnecessary.

On the other hand, negative refraction (NR), another anomalous refractive effect of PCs with negative dispersion relations, has also attracted much attention [20–23]. The physical principles allowing for NR in PCs arise from the dispersion characteristics in a periodic structure, which can be described by analyzing the equifrequency surfaces (EFSs) [20, 22] of the photonic band structures. If the direction of the group velocity is anti-parallel to the wave vector within the PC, a negative effective refractive index (NERI) can be defined [21]. In the past, NR was mainly investigated for subwavelength imaging, leading to various lensing-related applications [23, 24]. Very recently, it was demonstrated that collimated beams (i.e., DE) could also be achieved from a metallic PC with NERI [19]. The absorption loss of this metal PC is inevitable and a little power could be transferred into the collimated beams. We find that near the band-edge, the NERI of a dielectric PC can be very small in magnitude. This property could be used to realize highly DE with no absorption loss and greatly improved quality by properly designing the structure.

W.Y. Liang · J.W. Dong · G.Q. Liang · H.Z. Wang (✉)
State Key Laboratory of Optoelectronic Materials and Technologies, Zhongshan (Sun Yat-sen) University, Guangzhou 510275, People's Republic of China
e-mail: stswhz@mail.sysu.edu.cn
Fax: +86-20-84037423

In this paper, we demonstrate NR-based highly collimated emission from a build-in dipole source surrounded by a PC quasi-cavity. A quite narrow collimated beam with small half-power beam width (HPBW) is achieved. Besides, the HPBW of such a beam can be reduced by optimizing the size of the source area.

2 Structural analysis

Our structure consists of two dielectric PCs (PC-1 and PC-2) with different lattice constants, as depicted in Fig. 1. The quasi-cavity is a concave PC-1 mounted on the source area (i.e. the small area of PC-2). For the source area, N_x and N_y represent the period numbers of PC-2 along X-axis and Y-axis, respectively. PC-1 and PC-2 are both two-dimensional square lattices consisting of air holes (infinitely long in Z direction) introduced into a lossless dielectric medium with refractive index $n = 3.4$. The radii of air holes and lattice constants are r_1, a_1 and r_2, a_2 for PC-1 and PC-2, respectively. Throughout this paper, only H-polarization (magnetic field perpendicular to the X–Y plane) is studied. In order to satisfy the demand of our design, we choose the special relation $a_2 = 1.376a_1$ between the two lattice constants, while keeping the r/a ratio fixed, i.e., $r_1/a_1 = r_2/a_2 = 0.34$.

Due to the scaling law [25], the two PCs possess the same band structures as shown in Fig. 2a. The band structure is calculated by the plane wave expansion method [26] (using the free MPB software package provided by MIT). For convenience, all the referred frequencies in the following discussion are normalized to a_2. Figure 2a shows that two omnidirectional PBGs (regions 1 and 2) lie in the range 0.235–0.248 and 0.340–0.350, respectively, which ensures that only the modes of the second band can be excited (no band overlap). The operation frequency range 0.330–0.334 of PC-2 is denoted region 3. The corresponding EFS diagram (Fig. 2b) is also calculated by the plane wave expansion method. In PC, it has been proved that the direction of light propagation corresponds to the direction of the group velocity vector $\mathbf{v}_g = \nabla_k(\omega(\mathbf{k}))$ [25]. The group velocity vector $\mathbf{v}_g$ is always oriented perpendicular to the EFS in the direction along which $\omega(\mathbf{k})$ is increasing. Figure 2b shows that the EFS of PC-2 shrinks with increasing frequency; moreover, each EFS is nearly circular around the Γ point and has a small radius, suggesting that PC-2 can be regarded as an effective medium with small NERI over region 3. On the other hand, through the special relation $a_2 = 1.376a_1$, region 3 of PC-2 would lie within the first PBG (region 1) of PC-1. As a result, PC-1 will act as a reflector over the operation frequency range.

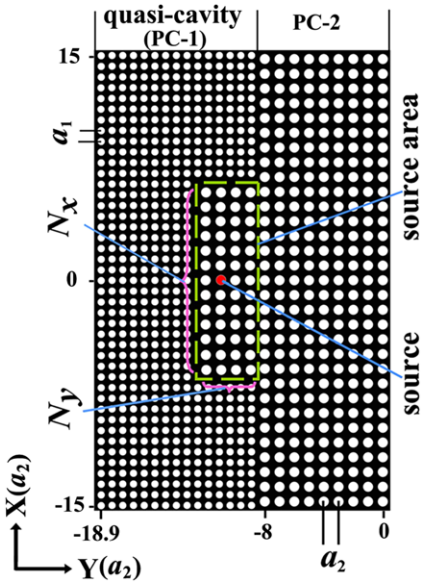

Fig. 1 Schematic sketch of the designed structure consisting of a PC-2 with NERI and a quasi-cavity (i.e., the concave PC-1). *The dashed rectangle* denotes the source area. An H-polarized dipole source is placed at $(-11a_2, 0)$

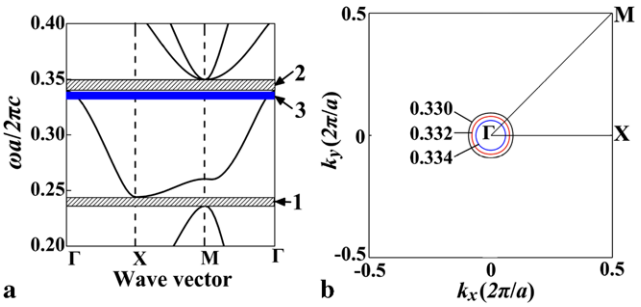

Fig. 2 **a** Band structure for H-polarization of PC-2 (also PC-1). Regions 1 and 2 denote two omnidirectional PBGs, while region 3 denotes the operation frequency range 0.330–0.334 of PC-2. **b** The EFS diagram of PC-2 within region 3. The radii of the EFSs are small and the direction of the group velocity is anti-parallel to the wave vector with PC-2, suggesting that NERIs can be defined within region 3

3 Physical mechanism analysis

Next, we discuss the physical mechanism on the highly collimated emission proposed in this paper. Figure 3 shows the schematic diagram for understanding the collimation phenomenon. A dipole source is placed within the source area. θ_1 is the incident angle and d is the source distance starting from the side AB.

Firstly, we discuss the propagation of EM wave within the designed structure. Detailed analysis shows that the ratio N_x/N_y, characterizing the size of the source area, is an optimization parameter to the collimation. As shown in Fig. 3, two parts of the dipole emissions have positive effects to the collimation: the forward wave and the backward wave un-

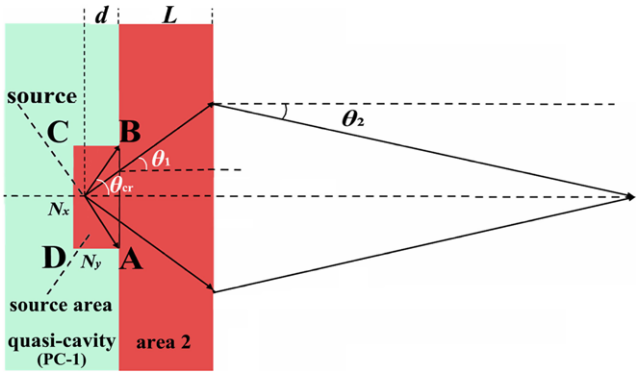

Fig. 3 Schematic diagram for understanding the collimation phenomenon. *The rectangle ABCD* denotes the source area. d and L are the source distance and the thickness of PC-2, respectively. A ray emitted from the source with an incident angle θ_1 is refracted with an angle θ_2 in air

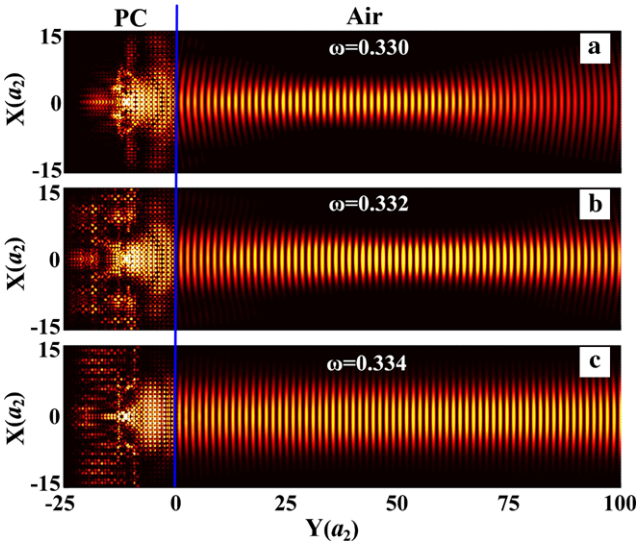

Fig. 4 The spatial distribution of the total magnitude of the Poynting vector at: **a** $\omega = 0.330$; **b** $\omega = 0.332$; **c** $\omega = 0.334$. The parameters are $N_x = 13$, $N_y = 4$, $d = 2.5a_2$, and $L = 8a_2$, respectively. *The blue vertical line* denotes the PC-air interface

dergoing single-trip reflection on the rear-side CD. Both of them are within the critical angle $\theta_{\rm cr} = \tan^{-1}[N_x a_2/(2d)]$. Therefore, one can decrease the ratio N_x/N_y, which is of advantage to collimating the output beam. On the other hand, the backward wave undergoing multi-trip reflections, as well as the wave reflected from the lateral sides (AD and BC), will enter area 2 with large angles. These two parts are unfavorable to the collimation. To reduce their contributions, one can increase the ratio N_x/N_y. Since the two aforementioned factors are competing, the ratio N_x/N_y should have an optimum value. Note that the ray-optical explanation above is valid in our design because of the isotropic EFS and the sufficiently large structural size compared to the wavelength [27].

Secondly, we investigate the NR behavior at the air-PC interface to show that the small NERI of PC-2 plays the most important role in the beaming. Figure 2b shows that with increasing frequency, the wave vector k_1 of PC-2 becomes smaller, but k_2 of air becomes larger from the dispersion relation $\omega = ck_2$ in air, resulting in significantly decreasing of the ratio k_1/k_2. By applying the continuity conditions of the transverse wave vectors across the interface [21], one can calculate the NERI of PC-2 by $n(\omega) = -k_1(\omega)/k_2(\omega)$. The calculated NERIs for $\omega = 0.330, 0.332$, and 0.334 are -0.198, -0.072, and -0.052, respectively. According to Snell's law, we get the refracted angle in air to be $\theta_2 = \sin^{-1}[n(\omega)\sin\theta_1]$. Due to the small magnitude of $n(\omega)$, the EM wave emitted from the build-in dipole source would be refracted into air with a small angle θ_2 even under the large incident angle θ_1. As a result, highly collimated emission with low angular divergence can be achieved. It should be noticed that the NERI at high frequency is much smaller than that at low frequency. This implies that the quality of the collimated beam at higher frequency will be much better than that at lower frequency.

4 Numerical simulations and optimization

In order to verify the prediction of the collimation phenomenon, we perform finite-different time-domain (FDTD) simulations with the perfectly-matched-layer boundary condition [28]. The spatial resolution Δx and Δy are set to be $\Delta x = \Delta y = a_2/32$. The time step Δt is given by Courant stability condition $\Delta t = S\Delta x/c \le (1/\sqrt{2})\Delta x/c$, where S is chosen as $1/2$ for the FDTD simulations to be stable. The parameters of the source area are $N_x = 13$ and $N_y = 4$ ($N_x/N_y = 3.25$), respectively. The thicknesses of PC-1 and PC-2 are $17a_2$ and $8a_2$, respectively. The dipole source is at $(-11a_2, 0)$, corresponding to a source distance $d = 2.5a_2$. FDTD simulations at $\omega = 0.330, 0.332$, and 0.334 are carried out, respectively. Figure 4 displays the spatial distributions of the total magnitude of the Poynting vector.

Figure 4 clearly shows that highly collimated emission is obtained. Additionally, it shows that a focus appears due to NR occurring at the air-PC interface. With increasing frequency, the focus shifts towards the far field and the corresponding HPBW becomes smaller (Fig. 5a). HPBW is the angular separation of the half-power points of the radiated pattern. It can be calculated through the exported data from the simulation results. The calculated HPBWs are $16.50°, 3.68°$, and $3.48°$ for $\omega = 0.330, 0.332$, and 0.334, respectively. The best collimated emission case is at $\omega = 0.334$, which maintains a high quality even at far field. It is noticed that the HPBW at $\omega = 0.330$ is much larger than those at higher frequencies due to the dispersion characteristics. Further calculations show that at lower frequency, the EFS distorts from a circle and its NERI is larger than that

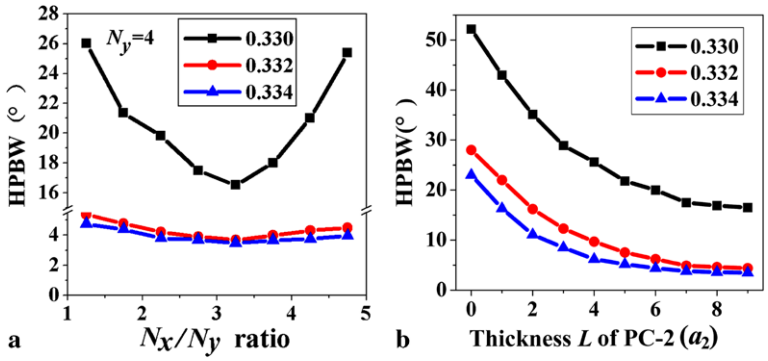

Fig. 5 **a** The HPBWs for different N_x/N_y ratios at $\omega = 0.330, 0.332$, and 0.334 respectively. **b** The HPBWs for different thickness L of PC-2

at higher frequency,resulting in more complicated distribution of the Poynting vector and a larger HPBW at lower frequency.

In order to achieve the best collimation result, the parameter N_x/N_y is optimized. The HPBW is used to characterize the quality of the collimated beam. Without loss of generality, we change N_x from 5 to 19 (by step 2), while keeping N_y fixed ($N_y = 4$) to get different N_x/N_y ratios. The calculated HPBWs are shown in Fig. 5a. It distinctly shows that as N_x/N_y increases, the HPBWs for these three frequencies first drop to minimum values and then ascend. The optimal value of N_x/N_y is 3.25 (i.e., $N_x = 13$ and $N_y = 4$). The corresponding HPBWs are 16.50°, 3.68°, and 3.48° for $\omega = 0.330, 0.332$, and 0.334, respectively. Having obtained the optimal ratio of N_x/N_y, the influence of the source distance d is investigated. Within the source area, the location of the source can take discrete values of $(-12a_2, 0)$, $(-11a_2, 0)$, $(-10a_2, 0)$, and $(-9a_2, 0)$. Detailed simulation results show that the best collimated results are achieved at $(-11a_2, 0)$, corresponding to a source distance $d = 2.5a_2$. In fact, Fig. 4 is just the distributions of the total magnitude of the Poynting vector under the above optimal parameters.

Furthermore, the role of the thickness L of PC-2 in the collimated emission is also considered. Figure 5b displays the HPBWs of the collimated beams with different L (from 0 to $9a_2$) under the aforementioned optimal parameters. When L is 0, the HPBWs for the three frequencies are very large, meaning that no collimated beams appear. With increasing L, the HPBWs drop rapidly and finally reach stable values after $L = 7a_2$. These results suggest that the Bragg scattering of the EM wave within a finite PC-2 of $L \geq 7a_2$ produces almost the same photonic band structure as an infinite PC-2. Therefore, it is reasonable to choose $L = 8a_2$ in the previous FDTD simulations to demonstrate the NR-based collimated emission.

5 Conclusion

In conclusion, we have demonstrated NR-based highly collimated emission from a NERI PC with a concave PC reflector. The numerical simulations show that a quite narrow collimated beam is achieved and the HPBW of such a beam can be reduced to 3.48° after optimizing the size of the source area. Further calculations show that PC-2 with thickness $L = 8a_2$ is suitable for demonstrating the NR-based collimated emission. Our designed structure exhibits advantages of high directivity and compact size. It can evidently improve the radiation characteristics of microwave antennas. Besides, it also holds promise for applications in the optical regime.

Acknowledgements This work was supported by the National Natural Science Foundation of China (10874250, 10674183, and 10804131), the National 973 Project of China (2004CB719804), and Ph.D. Degrees Foundation of Education Ministry of China (20060558068).

References

1. C.M. Anderson, K.P. Giapis, Phys. Rev. Lett. **77**, 2949 (1996)
2. J.W. Dong, H.Z. Wang, Appl. Phys. Lett. **91**, 111909 (2007)
3. A.R. Weily, K.P. Esselle, B.C. Sanders, Phys. Rev. E **70**, 037602 (2004)
4. H.J. Lezec, A. Degiron, E. Devaux, R.A. Linke, L. Martin-Moreno, F.J. Garcia-Vidal, T.W. Ebbesen, Science **297**, 820 (2002)
5. I. Bulu, H. Caglayan, E. Ozbay, Appl. Phys. Lett. **83**, 3263 (2003)
6. E. Moreno, F.J. García-Vidal, L. Martín-Moreno, Phys. Rev. B **69**, 121402 (2004)
7. P. Kramper, M. Agio, C.M. Soukoulis, A. Birner, F. Müller, R.B. Wehrspohn, U. Gösele, V. Sandoghdar, Phys. Rev. Lett. **92**, 113903 (2004)
8. S.K. Morrison, Y.S. Kivshar, Appl. Phys. Lett. **86**, 081110 (2005)
9. I. Bulu, H. Caglayan, E. Ozbay, Opt. Lett. **30**, 3078 (2005)
10. C.C. Chen, T. Pertsch, R. Iliew, F. Lederer, A. Tünnermann, Opt. Express **14**, 2423 (2006)
11. D. Tang, L. Chen, W. Ding, Appl. Phys. Lett. **89**, 131120 (2006)
12. Z.H. Zhu, W.M. Ye, J.R. Ji, X.D. Yuan, C. Zen, Appl. Phys. B **86**, 327 (2007)
13. Z. Li, K. Aydin, E. Ozbay, Appl. Phys. Lett. **91**, 121105 (2007)
14. S.K. Morrison, Y.S. Kivshar, Appl. Phys. B **94**, 149 (2009)
15. H. Kurt, Appl. Phys. B **95**, 341 (2009)
16. W.Y. Liang, J.W. Dong, H.Z. Wang, Opt. Express **15**, 1234 (2007)
17. Y. Zhang, Y. Zhang, B. Li, Opt. Express **15**, 9281 (2007)
18. J.M. Park, S.G. Lee, H.Y. Park, J.E. Kim, Opt. Express **16**, 20354 (2008)

19. M.A. Kaliteevski, S. Brand, R.A. Abram, A.J. Gallant, J.M. Chamberlain, Opt. Express **16**, 14582 (2008)
20. M. Notoni, Phys. Rev. B **62**, 10696 (2000)
21. S. Foteinopoulou, C.M. Soukoulis, Phys. Rev. B **67**, 235107 (2003)
22. S. Foteinopoulou, C.M. Soukoulis, Phys. Rev. B **72**, 165112 (2005)
23. E. Cubukcu, K. Aydin, E. Ozbay, S. Foteinopoulou, C.M. Soukoulis, Phys. Rev. Lett. **91**, 207401 (2003)
24. Z. Lu, C. Chen, C.A. Schuetz, S. Shi, J.A. Murakowski, G.J. Schneider, D.W. Prather, Appl. Phys. Lett. **87**, 091907 (2005)
25. K. Sakoda, *Optical Properties of Photonic Crystals* (Springer, New York, 2001)
26. S.G. Johnson, J.D. Joannopoulos, Opt. Express **8**, 173 (2001)
27. X. Wang, Z.F. Ren, K. Kempa, Opt. Express **12**, 2919 (2004)
28. A. Taflove, S.C. Hagness, *Computational Electrodynamics: The Finite-Difference Time-Domain Method*, 2nd edn. (Artech House, Boston, 2000)